Atmospheric Environment 44 (2010) 4014–4023

Contents lists available at ScienceDirect

Atmospheric Environment

journal homepage: www.elsevier.com/locate/atmosenv

Nocturnal boundary layer characteristics and land breeze development in Houston, Texas during TexAQS II

Bridget M. Day [a], Bernhard Rappenglück [a,*], Craig B. Clements [a,1], Sara C. Tucker [b,c], W. Alan Brewer [c]

[a] Department of Earth and Atmospheric Sciences, University of Houston, 4800 Calhoun Rd, Houston, TX 77204-5007, USA
[b] Cooperative Institute for Research in Environmental Sciences, University of Colorado at Boulder, 325 Broadway, Boulder, CO 80305, USA
[c] NOAA Earth System Research Laboratory, 325 Broadway, Boulder, CO 80305, USA

ARTICLE INFO

Article history:
Received 4 September 2008
Received in revised form
14 January 2009
Accepted 25 January 2009

Keywords:
TexAQS II
Tethersonde
Urban nocturnal boundary layer
Inversion height
Land breeze

ABSTRACT

The nocturnal boundary layer in Houston, Texas was studied using a high temporal and vertical resolution tethersonde system on four nights during the Texas Air Quality Study II (TexAQS II) in August and September 2006. The launch site was on the University of Houston campus located approximately 4 km from downtown Houston. Of particular interest was the evolution of the nocturnal surface inversion and the wind flows within the boundary layer. The land–sea breeze oscillation in Houston has important implications for air quality as the cycle can impact ozone concentrations through pollutant advection and recirculation. The results showed that a weakly stable surface inversion averaging in depth between 145 and 200 m AGL formed on each of the experiment nights, typically within 2–3 h after sunset. Tethersonde vertical winds were compared with two other Houston data sets (High Resolution Doppler Lidar and radar wind profiler) from locations near the coastline and good agreement was found, albeit with a temporal lag at the tethersonde site. This comparison revealed development of a land breeze on three nights which began near the coastline and propagated inland both horizontally and vertically with time. The vertical temperature structure was significantly modified on one night at the tethersonde site after the land breeze wind shift, exhibiting near-adiabatic profiles below 100 m AGL.

1. Introduction

The Houston metropolitan area in southeast Texas is a non-attainment region under United States federal ozone standards and development of an effective pollution control strategy for the region is ongoing. Although progress has been made in improving air quality, continued economic and population growth in the Houston area creates additional challenges. In March 2008, the United States Environmental Protection Agency (EPA) lowered the primary standard for 8-h average ozone levels from 84 parts per billion (ppbv) to 75 ppbv (EPA, 2008), further complicating the region's issues.

The Texas Air Quality Study II (TexAQS II) was conducted in August and September 2006 and was designed to collect a comprehensive data set of chemical and meteorological observations to further the understanding of urban pollution formation and transport in eastern Texas, including the greater Houston area. The goals of the research discussed here are to increase the current understanding of the nocturnal planetary boundary layer (NBL) and nighttime wind flows in Houston through observations taken during TexAQS II. Collected primarily via tethersonde, this high resolution data set (both temporally and vertically) provides information about the NBL evolution in an urban area on four nights, including the height of the boundary layer (BL), the near-surface atmospheric stability, and the effect of wind flows on the NBL structure. To our knowledge, few other nocturnal data sets of vertical meteorological profiles exist for this area. Those sets include Doppler radar wind profiles from the La Porte airport (during TexAQS II and TexAQS-2000) and High Resolution Doppler Lidar and rawinsondes from the NOAA Research Vessel Ronald H. Brown (Ron Brown) (during TexAQS II) (J. Nielsen-Gammon, personal communication, 2008).

The BL height determines the volume available for dispersion of pollutants released at the surface, therefore it is a key input to air quality models. Within the BL, the atmospheric stability and wind structure influence the spatial and temporal extent of the pollutant mixing. Currently, the ability to reliably determine the height of the BL under all conditions is an unsolved scientific problem (Seibert

* Corresponding author. Tel.: +1 713 743 1834; fax: +1 713 748 7906.
E-mail address: brappenglueck@uh.edu (B.M. Day).
[1] Present address: Department of Meteorology, San José State University, One Washington Square, San José, CA 95192, USA.

1352-2310/$ – see front matter
doi:10.1016/j.atmosenv.2009.01.031

et al., 2000) and thus modelers are left with imperfect parameterizations. The NBL typically belongs to the category of stable BLs, which are particularly challenging to parameterize and test because they vary in structure and duration and are difficult to observe (Teixeira et al., 2008). Also, the NBL evolution in an urban area is more complex than in a rural area because the urban NBL is influenced by mechanical and thermal turbulence generated by roughness elements such as buildings, different radiative properties of heterogeneous surfaces, and anthropogenic heat sources (Oke, 1978; Dabberdt et al., 2004).

The definition of the NBL is extensively discussed in the literature. For example, Berman et al. (1999) and Seibert et al. (2000) characterize the NBL as composed of two sections – the near-surface layer with continuous turbulence and a higher layer of intermittent turbulence. The near-surface layer is termed the mixing height and the top of the second layer coincides with the top of the nocturnal surface temperature inversion (NSI). André and Mahrt (1982) note that the NSI develops due to a cooling ground surface, clear-air radiative cooling, and horizontal advection. Berman et al. (1999) discuss the NSI as the "upper boundary on the air's dispersive ability at night" over a highly urbanized area and note that although the turbulence above the mixing height may be weak and sporadic, pollutants may slowly disperse throughout the stable layer capped by the NSI.

Houston's coastal location and complex coastline (incorporating Galveston Bay and the Gulf of Mexico) also complicate urban BL dynamics through a diurnal land–sea breeze oscillation created by thermal forcing between the land and the water (Banta et al., 2005; Darby, 2005). As discussed in Banta et al. (2005), the Coriolis force turns the wind vector steadily clockwise in the lower levels over the 24-h heating and cooling cycle; this cycle is near maximum amplitude in Houston due to its location at 30° North latitude. The land breeze portion of the oscillation is one focus of this study, in particular how it propagates across the area and interacts with the NBL structure. A Houston land breeze is defined here as offshore flow from the northwest or north, whereas bay and sea breeze references encompass east–southeast to south onshore winds. Two studies in east-central Florida found nocturnal land breezes which formed inland and moved to the coastline (Zhong and Takle, 1992; Case et al., 2005). In contrast, initial land breeze formation near the coastline was noted in a numerical simulation of a flat coastal urban environment at 45° North latitude (Martilli, 2003).

During periods of weak synoptic flow, this local-scale land–sea breeze cycle can dominate Houston's meteorology and affect air quality through pollutant advection and recirculation. Land–sea breeze recirculation impacts on air quality have been found in other coastal cities such as Athens, Greece (Clappier et al., 2000; Grossi et al., 2000) and Los Angeles, California (Lu and Turco, 1996). Topography also plays an important role in the oscillation; for example, Houston's flat coastal plain allows the winds to rotate through the entire diurnal cycle without interference from nearby mountains as found in Athens and Los Angeles.

In Houston, northwesterly offshore flow overnight can advect previous-day and current-morning ozone and ozone precursors over Galveston Bay or the Gulf of Mexico. As the oscillation continues, winds turn easterly later in the morning, advecting industrial emissions from the Houston Ship Channel's petrochemical and refinery complexes into the metropolitan area (Rappenglück et al., 2008). Subsequent onshore bay or sea breeze development can return the pollutants advected earlier over the water to the city where they may combine with local emissions to significantly impact ozone production and concentrations during the afternoon. Banta et al. (2005) discuss an August recirculation pollution episode in Houston during TexAQS-2000 through an in-depth case study. An additional TexAQS-2000 analysis found that significant spatial variations in the daytime mixing height exist throughout the Houston area (Nielsen-Gammon et al., 2008), which may further complicate air quality conditions. These two TexAQS-2000 analyses (and also Darby, 2005), primarily address daytime observations; there has not yet been a focused study on nighttime boundary layer conditions.

2. Methods

2.1. Site description

The vertical sounding experiment site was on the University of Houston campus (UH), centrally located approximately 4 km southeast of downtown Houston (Fig. 1). UH has an elevation of 11 m above sea level and is comprised of 2.2 km^2 of flat terrain with a mix of low to mid-rise buildings, trees and other vegetation, and asphalt parking lots. The only high-rise buildings on campus are the 18-story (65 m) Moody Tower dormitories located 0.75 km south of the launch site. The launch site was surrounded by parking lots, several one-story trailers to the northeast, and a sparse mix of grass and trees. Although the launch site was located close to the city center, the campus environment lent a more suburban feel as compared with a downtown site with a dense group of high-rise buildings.

2.2. Instrumentation and measurements

Vaisala, Inc.'s DigiCora III Tethersonde System was used for the experiments. All the soundings were taken consecutively in profile mode using the same TTS-111 tethersonde. Meteorological parameters (atmospheric pressure, ambient/potential temperature, relative humidity, and wind speed/direction) were measured at 1 Hz with the tethersonde's HUMICAP®, BAROCAP®, and THERMOCAP® sensors, and a cup anemometer. The sonde ascent rate averaged 1–2 m s^{-1}.

Soundings were performed on four overnight periods in 2006: August 31–September 1, September 1–2, September 7–8, and September 14–15. The measurement periods coincided with the

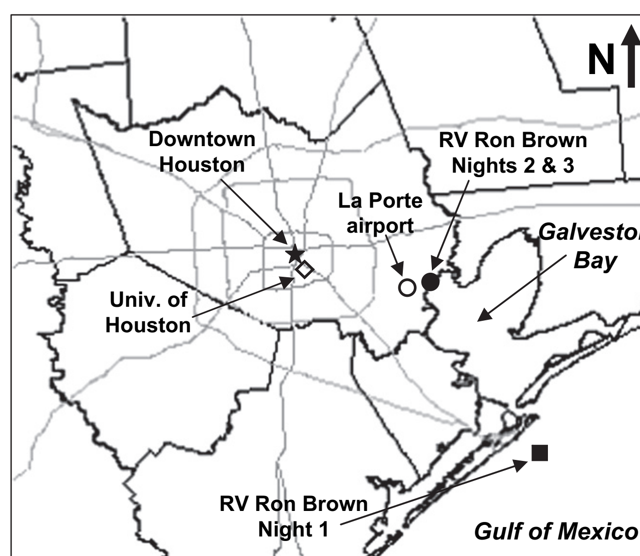

Fig. 1. Map of Houston, Texas metropolitan area. Locations of interest are marked as follows: downtown central business district (star), University of Houston campus (tethersonde and rawinsonde launch site, open diamond), La Porte radar wind profiler (open circle), NOAA Research Vessel Ronald H. Brown on night 1 (square) and nights 2 and 3 (closed circle).

TexAQS II campaign's Intensive Observational Periods (IOPs) during which Houston was expected to experience 8-h average ozone concentrations greater than 84 ppbv.

Tethersonde measurements were taken at varying intervals from approximately 2000 CST (central standard time) through the following morning. However, on September 1–2 the soundings did not begin until after 2300 CST. Vertical profile heights averaged 250 m above ground level (AGL), with a few profiles up to 400 m AGL. A total of 161 tethersonde soundings were taken during the campaign and half of these are associated with the overnight periods.

To increase the temporal coverage of vertical profiles, the tethersonde data set was supplemented by soundings taken with Vaisala, Inc. RS-92-SGP rawinsondes. The rawinsondes were launched during IOPs from the same site at UH at 2100, 0000, 0400, and 0600 CST and averaged ascent rates of 5 m s^{-1} with a 0.5-Hz data capture rate.

2.3. Data processing

The NBL heights discussed here are the observed heights of the NSI because turbulence measurements were not taken at the observation site during the overnight experiments. Other NBL height determination methods were also considered in the analysis: height of the low-level wind maximum, height where Richardson number exceeded a critical value, and height at which relative humidity (or water vapor mixing ratio) exhibited clear discontinuity (André and Mahrt, 1982; Berman et al., 1999). All four methods may yield a different NBL height for the same profile because each parameter's vertical structure is influenced differently by processes occurring at the surface and in the atmosphere (see Seibert et al., 2000). Overall, the NSI height method was superior in yielding more consistent results across all profiles. A shortcoming of this method included difficulty identifying a clear top to the inversion layer because cooling occurred throughout the troposphere. Also, unlike the Richardson number analysis, the NSI method did not incorporate mechanical and thermal turbulence into the NBL height determination. A bulk Richardson number analysis was conducted as well, but the results were uncertain.

NSI height was determined using virtual potential temperature (θ_v) profiles, and vertical sounding data were averaged into 5-m layers for analysis. Potential temperature removes the dry adiabatic temperature change experienced by air parcels as they are lifted and allows the stability of an air layer to be more easily determined which is key when considering diffusion of pollutants (Oke and East, 1971). θ_v adjusts the data further to remove the effects of water vapor on air density (important in a very humid location such as Houston). θ_v was used instead of equivalent potential temperature because no condensation occurred during ascent.

Because the NSI height was not clear-cut, we identified an elevated layer or range within which the NSI top was likely to reside, bracketing the inversion top. The range midpoint was set as the NSI height for analysis. To determine the elevated range, subjective visual inspection was coupled with objective calculations of the vertical θ_v gradient ($d\theta_v dz^{-1}$) over running 30-m layers. Within each vertical profile, near-zero values of $d\theta_v dz^{-1}$ (representing slightly stable or neutral layers) were used to set the upper

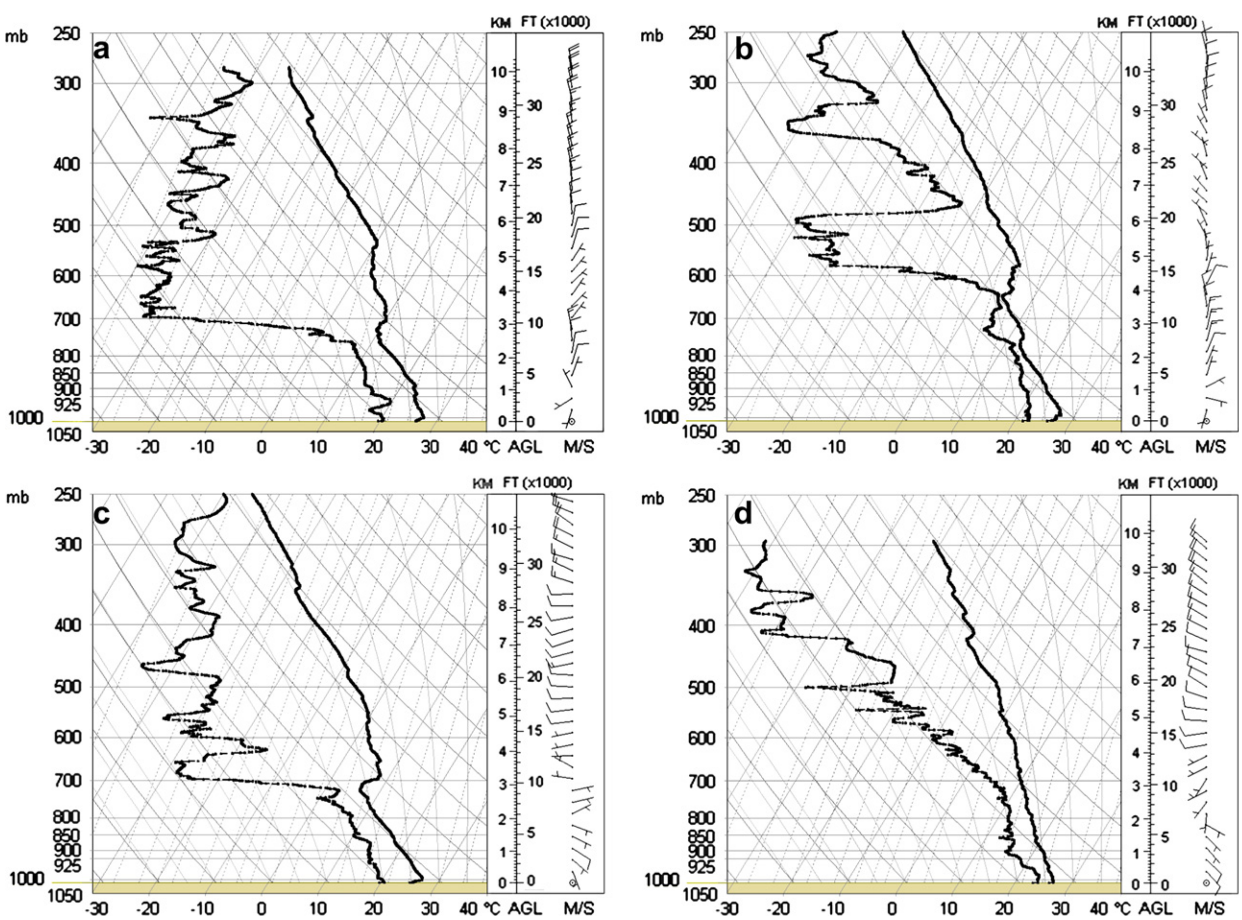

Fig. 2. Skew-T diagrams from 0000 CST rawinsonde soundings (launched from University of Houston campus): (a) night 1 (August 31–September 1, 2006), (b) night 2 (September 1–2, 2006), (c) night 3 (September 7–8, 2006), and (d) night 4 (September 14–15, 2006). Right line is temperature and left line is dew point temperature.

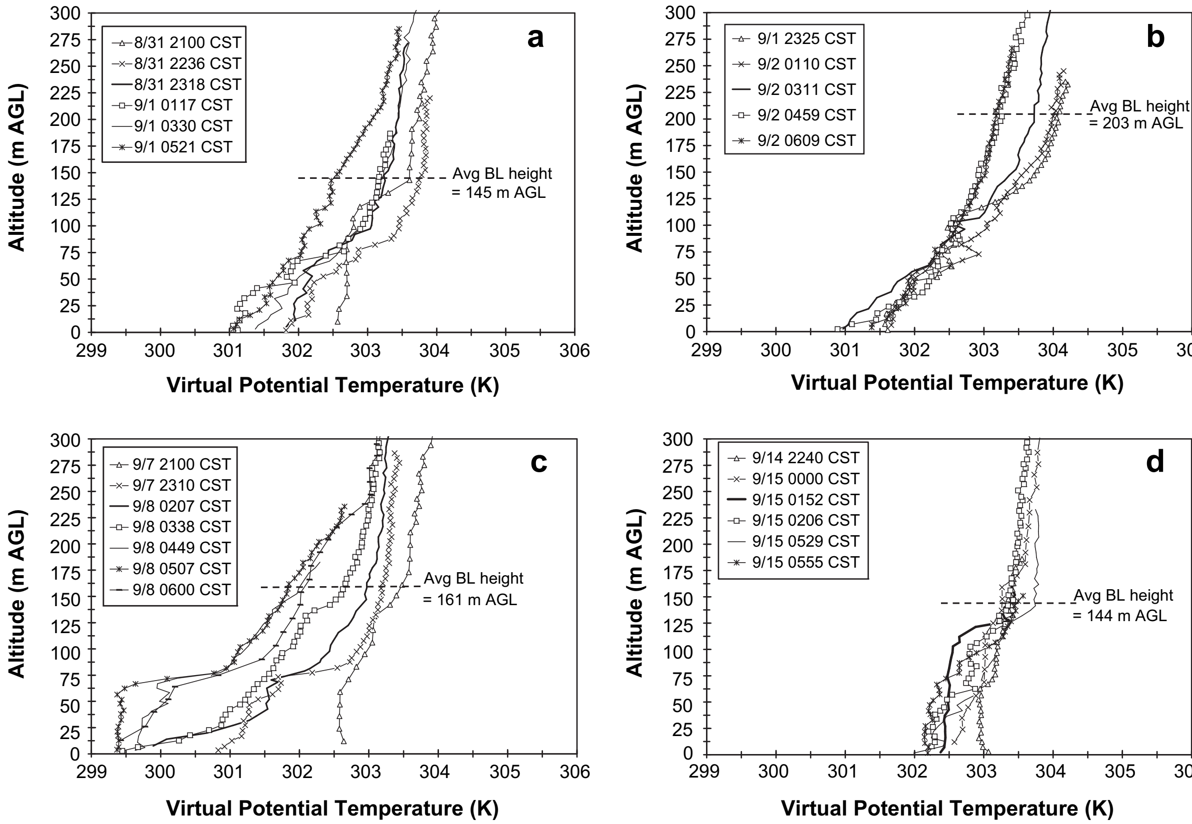

Fig. 3. Vertical profiles of virtual potential temperature from selected tethersonde and rawinsonde soundings for each night: (a) night 1 (August 31–September 1, 2006), (b) night 2 (September 1–2, 2006) (note that first sounding did not occur until 2325 CST, 3–4 h later than first sounding on other nights), (c) night 3 (September 7–8, 2006), and (d) night 4 (September 14–15, 2006). The horizontal dashed line represents the average nocturnal surface inversion height for each night.

and lower limits of the range. Visual inspection and comparison of previous and subsequent profiles were then used to fine-tune the range for each profile.

2.4. Comparison data sets

On three of the nights, High Resolution Doppler Lidar (HRDL) vertical wind profiles were available from the Ron Brown to compare with the tethersonde data. The ship was located in the Gulf of Mexico just off Galveston Island on night 1, and during nights 2 and 3 the ship was located in Barbour's Cut at the head of Galveston Bay (32 km east–southeast from UH) (Fig. 1). The HRDL, built by NOAA Earth System Research Laboratory, is a 2-μm wavelength coherent Doppler lidar used to measure lower-tropospheric winds in clear-air conditions (Grund et al., 2001). During TexAQS II, the HRDL performed continuous scanning measurements of BL winds and relative aerosol backscatter. The 30 m range-resolved lidar velocity and backscatter data were used to derive 15-min profiles of BL horizontal mean wind speed and direction and other products from the surface up through the top of the aerosol BL.

On all four nights, vertical wind profiles from the Texas Commission on Environmental Quality's 915-MHz radar wind profiler located at the La Porte, Texas airport were available for comparison to the tethersonde data. The La Porte site was located just west of Galveston Bay, 27 km from UH towards the east–southeast (Fig. 1). Temporal resolution of the data set was 1 h, the wind profiler minimum height was 128 m AGL, and height resolution was 58 m (W.M. Angevine, personal communication, 2008). Therefore, it was only compared with the tethersonde at 128 m AGL and above.

Table 1
Summary of nocturnal surface inversion and other statistics for experiment nights in 2006.

	August 31–September 1	September 1–2	September 7–8	September 14–15
Sunset (CST)	1845	1844	1837	1828
Sunrise (CST)	0559	0559	0602	0606
Inversion first apparent in temperature profiles (CST)	2100	2325[a]	2100	2240
Mean surface inversion height (m AGL)	145	203	161	144
Standard deviation of inversion height (m)	60	47	48	32
Range of inversion heights overnight (m AGL)	99–285	142–257	98–237	98–210
Peak inversion strength (θ_v, in K)	2.3	2.7	3.3	1.6
Inversion gradient at peak inversion strength (K m^{-1})	0.008	0.010	0.016	0.012
Peak inversion time (CST)	0600	0525	0600	0529
Mean water vapor mixing ratio in the vertical (g kg^{-1})	14.4	16.9	14.3	18.1

[a] The first sounding was conducted at this time, 3–4 h later than the first sounding on other nights presented.

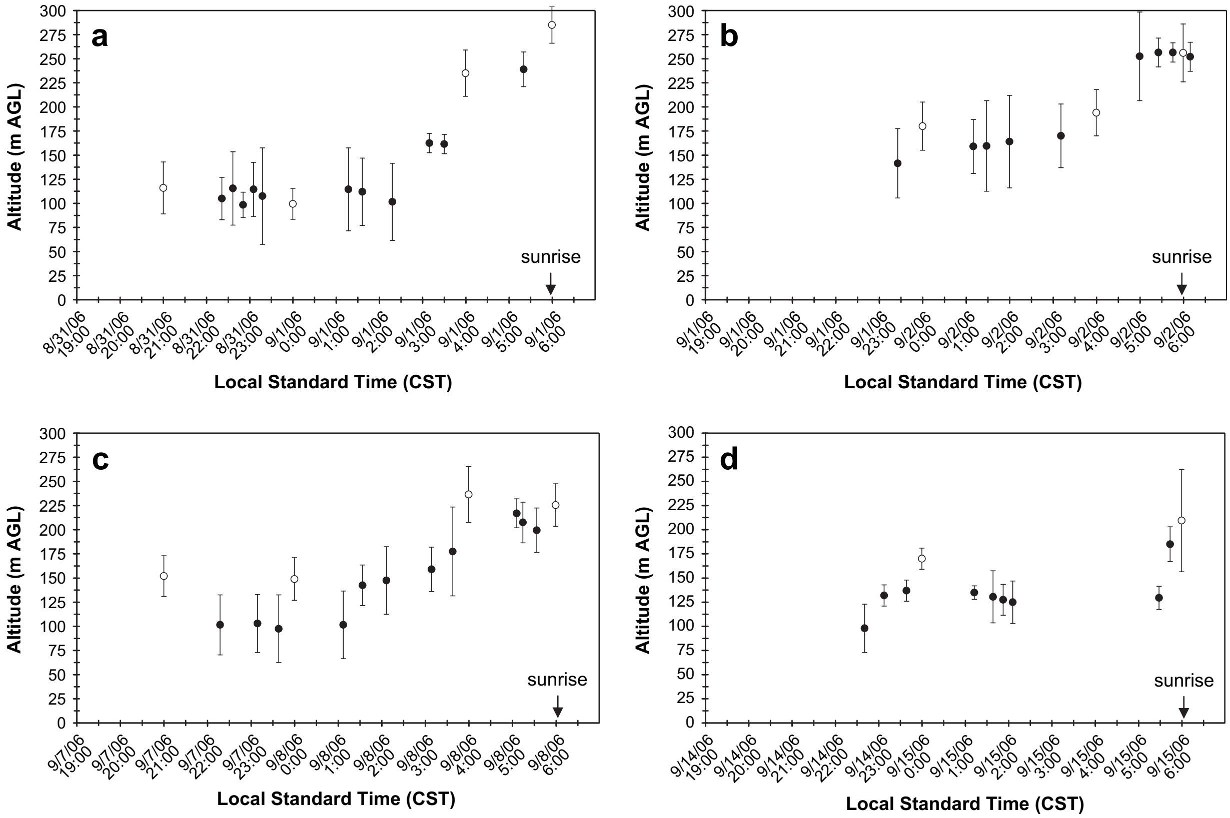

Fig. 4. Evolution of nocturnal surface inversion height for each night as derived from tethersonde and rawinsonde vertical profiles of virtual potential temperature: (a) night 1 (August 31–September 1, 2006), (b) night 2 (September 1–2, 2006), (c) night 3 (September 7–8, 2006), and (d) night 4 (September 14–15, 2006). Error bars reflect range in which inversion height resides, with circle indicating midpoint of range. Filled circles indicate tethersonde data and open circles indicate rawinsonde data.

2.5. Possible study limitations

Due to UH's proximity to Houston's Hobby Airport, the height of the tethersonde was restricted to the lowest part of the troposphere by the Federal Aviation Administration regulations. Therefore, some soundings were not able to reach the top of the NSI based on our height determination procedure. In most of the soundings, θ_v continuously increased with height within the troposphere, a not uncommon occurrence as discussed in Mahrt et al. (1982) and Dabberdt et al. (2004). As a result, discerning the top of the NSI was challenging and it is possible that our identification of the NSI top was too low because of the limited vertical reach of the instrument. Additionally, the rawinsonde soundings used to supplement the data set had coarser vertical resolution and lacked the fine-scale features of the tethersonde profiles, making the identification of the NSI height from these soundings more difficult.

Because the overnight soundings were conducted only on IOP days, the synoptic conditions were fairly similar (see Section 3.1) and the results may only reflect NBL development under these specific meteorological circumstances. Reference soundings were not conducted during other overnight periods, such as ones with stronger winds, to provide measurements for comparison.

3. Results

3.1. Synoptic overview

Synoptic conditions during all four overnight periods were influenced by the passage of cold fronts through Houston within the previous 48–72 h. Synoptic forcing on all these nights was weak and tethersonde mean wind speeds in the lowest 50 m AGL were light, averaging 1–2.5 m s^{-1} from 2300 to 0300 CST and 1–2 m s^{-1} from 0300 to 0600 CST.

On night 1 (August 31–September 1) and night 2 (September 1–2), the Houston area was to the east of a 500-hPa geopotential height ridge axis, and upper-level winds were northerly. At the surface, a center of high pressure was due south of Houston on both nights; it was along the Texas coastline on night 1 and in the Gulf of Mexico on night 2. On night 3 (September 7–8), the surface pressure gradient was very weak, Houston was to the east of a minor 500-hPa geopotential height ridge axis, and upper-level flows were zonal from the west. Night 4 (September 14–15) also had weak 500-hPa ridging to the west of Houston and westerly zonal flow at upper levels, but surface conditions were different than the other nights – a meridional pressure gradient over the Great Plains and a large dome of surface high pressure northeast of Texas created light onshore flow from the Gulf of Mexico.

The rawinsonde profiles revealed that night 1 had significant upper-level subsidence from a capping inversion structure (Fig. 2a). The first inversion was at 700 hPa (3.2 km), accompanied by very dry air. This inversion remained in place on night 2 (Fig. 2b), but it had ascended to about 575 hPa (4.8 km) and weakened as evidenced by its slightly moister air. Similar upper-level subsidence was in place on night 3 (Fig. 2c), although the air was not as dry as on night 1. The lowest cap was again at 700 hPa (3.2 km). On night 4, there was no significant capping inversion (Fig. 2d).

Mostly clear skies prevailed on night 1, while nights 2 and 3 had broken high clouds (ceiling at least 7600 m per METARs from Hobby Airport). Night 4 was mostly clear until 0500 CST when scattered and broken low clouds (750–900 m) were present. Mean water vapor mixing ratios varied in the sampled vertical columns for each night depending on how rapidly the drier air behind the

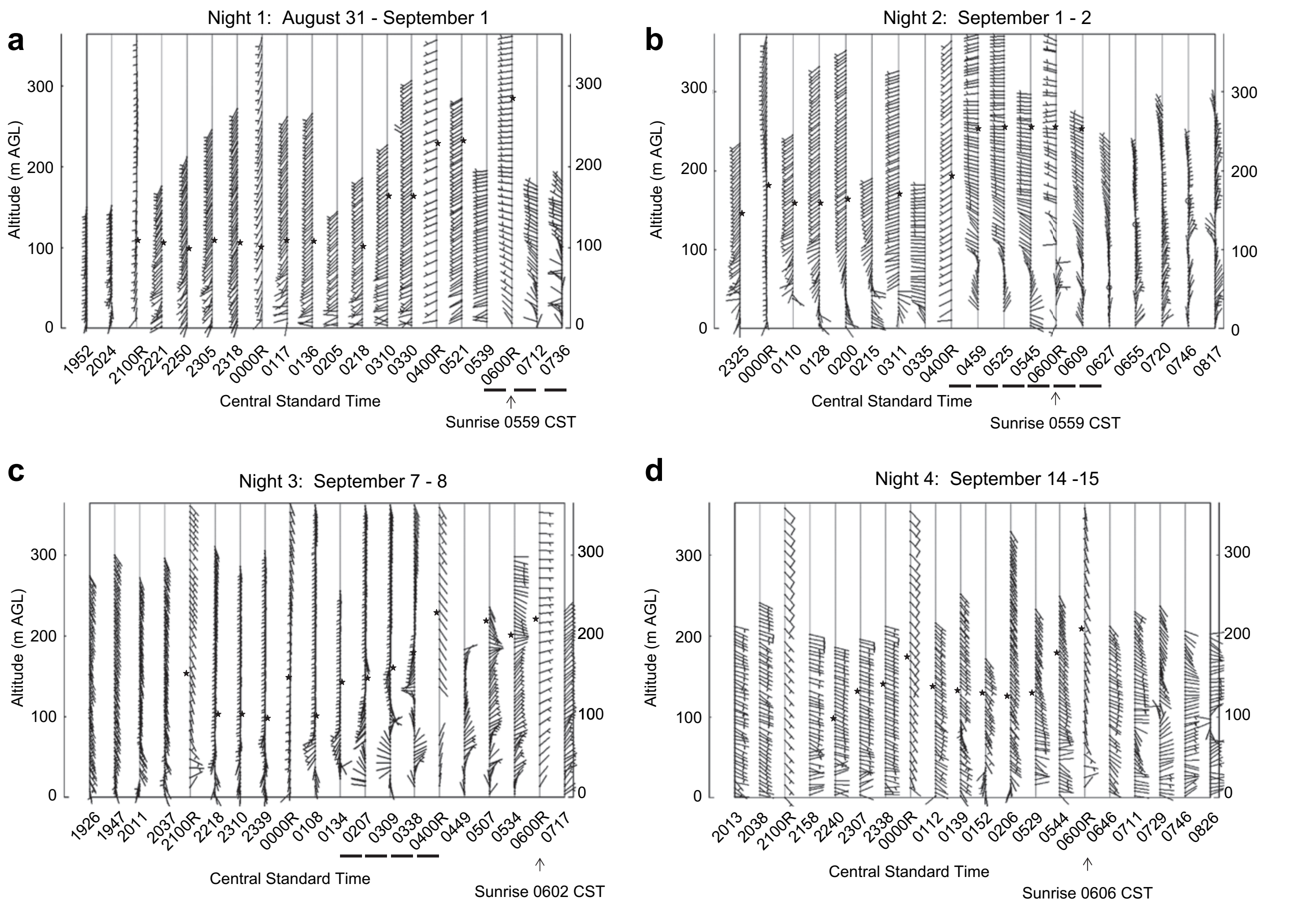

Fig. 5. Tethersonde and rawinsonde vertical wind profiles for each night: (a) night 1 (August 31–September 1, 2006), (b) night 2 (September 1–2, 2006), (c) night 3 (September 7–8, 2006), and (d) night 4 (September 14–15, 2006). Winds are in m s^{-1} and barbs point into the wind. A full feather indicates wind speeds of 8–12 m s^{-1}, a half feather equals 3–7 m s^{-1}, no feather is <3 m s^{-1}, and a circle is calm winds. Rawinsonde profiles are indicated by an "R" following the profile time. Black star on each profile indicates nocturnal surface inversion height. Black bars underneath the time represent land breeze profiles.

cold front moved off to the east. Nights 1 and 3 had air masses averaging 14 g kg^{-1} of water vapor (per kg of dry air), while nights 2 and 4 experienced more humid conditions with ratios averaging 17 g kg^{-1} and 18 g kg^{-1}, respectively.

3.2. Nocturnal surface inversion height

Previous studies of the NBL in urban locales have found unstable and neutral near-surface layers capped by elevated temperature inversions, e.g. in Minneapolis – St. Paul (Baker et al., 1969), Cincinnati (Clarke, 1969), Montreal (Oke and East, 1971), and St. Louis (Godowitch et al., 1985). Several of the Houston soundings exhibited near-adiabatic lower layers, but primarily our tethersonde results more closely resembled the stable or weakly stable near-surface layers observed in urban studies conducted in Pune, India (Vernekar et al., 1993), Hanover, Germany (Emeis and Türk, 2004), Basel, Switzerland (Rotach et al., 2005), Helsinki, Finland (Eresmaa et al., 2006), and Washington, D.C. (Frehlich et al., 2006).

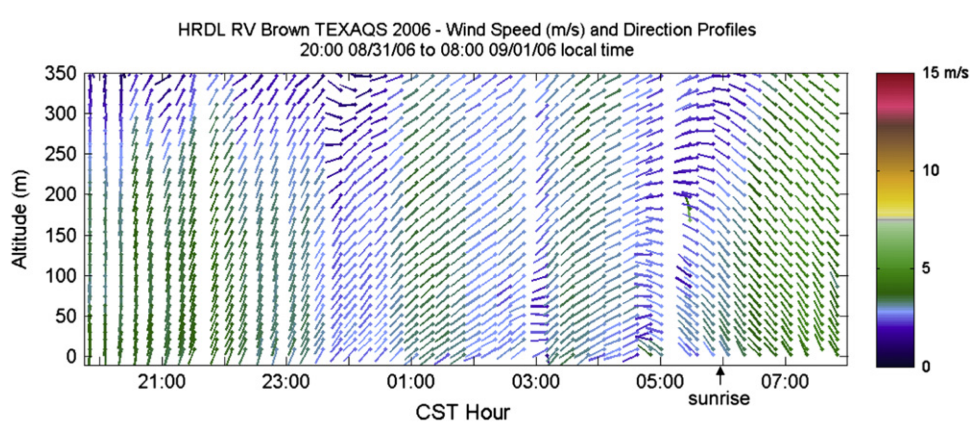

Fig. 6. Vertical mean wind profiles from NOAA High Resolution Doppler Lidar from 2000 to 0800 CST for night 1 (August 31–September 1, 2006). Winds are in m s^{-1}, barbs point into the wind, and color scale indicates speeds. (For interpretation of the references to color in this figure legend, the reader is referred to the web version of this article).

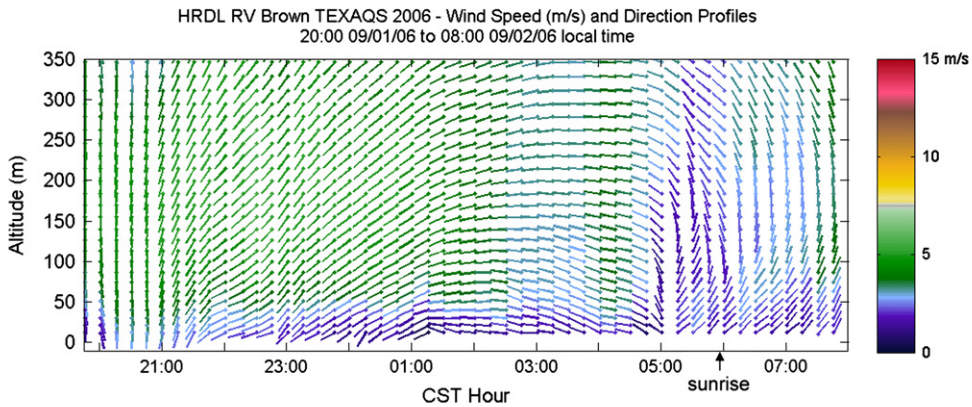

Fig. 7. Vertical mean wind profiles from NOAA High Resolution Doppler Lidar from 2000 to 0800 CST for night 2 (September 1–2, 2006). Winds are in m s^{-1}, barbs point into the wind, and color scale indicates speeds. (For interpretation of the references to color in this figure legend, the reader is referred to the web version of this article).

We attribute the NSI development to the open urban canopy environment of the launch site which allowed more efficient surface cooling to occur versus at denser urban sites.

On all four nights an NSI developed, capped by a near-neutral residual layer. Fig. 3 shows selected θ_v profiles for each night. Similar to the findings in Godowitch et al. (1985), the inversion developed within 2–3 h after sunset ($\sim$1840 CST), although on night 4 it did not form until 4 h after sunset. The mean NSI heights for nights 1, 2, 3, and 4 were 145 m, 203 m, 161 m, and 144 m, respectively, and as expected the peak inversion strength occurred at or right before sunrise ($\sim$0600 CST), varying from 1.6 K to 3.3 K (measured as θ_v difference between surface and NSI top). Although wind speed differences were slight among the nights, the mean inversion height was greater and the inversion was stronger on nights 2 and 3 which had the lowest mean wind speeds below 200 m AGL, indicating less mechanical mixing. Table 1 provides NSI statistics in more detail for each night.

The NSI temporal evolution followed a similar pattern each night with a fairly steady inversion height for several hours after formation (Fig. 4). But, it is interesting to note that the NSI height subsequently increased during the hours before sunrise, generally between 0300 and 0600 CST. This visual effect was confirmed through an objective calculation of the rate of increase in NSI height (in m min^{-1}) in order to remove any bias in the data set due to irregular sounding intervals.

The influence of urban thermal and mechanical turbulence can be seen on two of the nights in several vertical θ_v profiles with near-adiabatic layers below 100 m AGL. The high resolution tethersonde captured these structures more effectively than the rawinsondes. On night 3, these layers were present in the 0449 and 0507 CST soundings (Fig. 3c), and appear to have resulted from an abrupt wind shift advecting a cooler air mass above the surface and enhanced vertical mixing from increased wind speed (see Section 3.3). The development of these near-adiabatic structures also coincided with an increase in the NSI height.

The other near-adiabatic layers occurred on night 4 and can be seen in soundings taken at 0152 and 0555 CST (Fig. 3d). The NSI evolution was unique on this night relative to the other three – the NSI took longer to form and surface cooling was limited, resulting in a weak inversion (Fig. 4d). The main differences on this night were synoptically driven onshore flow, more abundant atmospheric water vapor present in the vertical column, and morning low cloud formation. The mean wind speeds in the lowest 200 m AGL were similar to the speeds on night 1 (and less than 2 m s^{-1} faster than nights 2 and 3), so greater mechanical turbulence does not seem to be the cause of the weak inversion. A potential reason for the lack of surface cooling is the interaction of outgoing longwave radiation (OLR) released from the urban surfaces around the launch site with the atmospheric water vapor and clouds. Atmospheric water vapor and cloud droplets can absorb OLR and re-radiate it towards the surface, limiting the extent of surface cooling (Ha and Mahrt, 2003).

We also analyzed the synoptic conditions above the BL to see if correlations existed between them and the various NSI

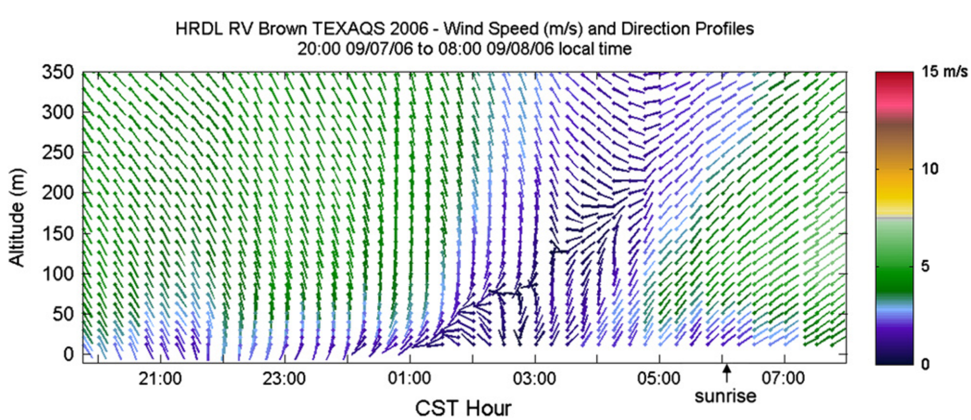

Fig. 8. Vertical mean wind profiles from NOAA High Resolution Doppler Lidar from 2000 to 0800 CST for night 3 (September 7–8, 2006). Winds are in m s^{-1}, barbs point into the wind, and color scale indicates speeds. (For interpretation of the references to color in this figure legend, the reader is referred to the web version of this article).

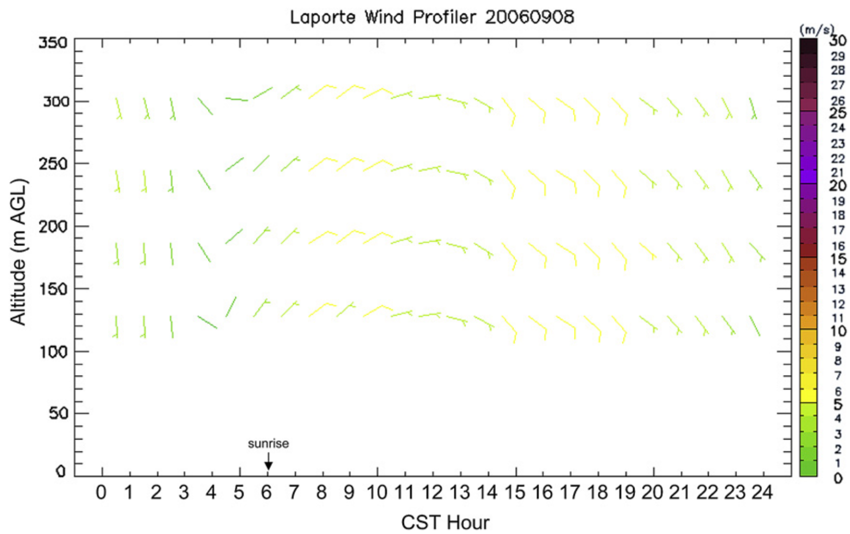

Fig. 9. Vertical wind profiles from La Porte airport radar wind profiler from 0000 to 2359 CST on night 3 (September 8, 2006). Winds are in m s^{-1}, barbs point into the wind, and color scale indicates speeds. (For interpretation of the references to color in this figure legend, the reader is referred to the web version of this article).

characteristics on different nights (such as NSI strength or height). This analysis revealed no obvious correlation between the inversion characteristics and the parameters such as upper-level subsidence, strong directional wind shear below 1 km, or upper-level wind direction and speed.

3.3. Vertical wind structure

This section discusses the vertical wind structure evolution on each night at the UH launch site. On night 1 (Fig. 5a), Houston's diurnal wind oscillation was evident in the tethersonde data with winds throughout the profiles veering with time from south to southwest (by 2230 CST) and continuing to west–southwest through 0530 CST. By 0600 CST, an apparent land breeze had developed in the lower 100 m AGL with winds from the northwest. The winds above became northwesterly also shortly after 0700 CST. Before midnight, wind speeds in the BL ranged from 2.5 m s^{-1} near the surface to 7 m s^{-1} at 200 m AGL. Between midnight and sunrise (0559 CST), wind speeds weakened at all levels but maintained the increase with height, peaking between 5 and 7 m s^{-1} near the top of the inversion.

On night 2 (Fig. 5b), the winds also exhibited the land–sea breeze circulation, but the cycle was more consistent above 100 m AGL than below. This was due to the weak wind speeds (less than 2 m s^{-1}) in the lower 100 m AGL between midnight and sunrise (0559 CST) and frictional effects in this layer from the urban landscape. The northwesterly land breeze onset can be seen in this lower layer in the 0459 CST sounding, but the winds were variable after that before they turned consistently northwesterly and northerly between 0600 and 0630 CST. Above 100 m AGL, however, wind direction veered smoothly through southwest and west, shifting to a northwest land breeze around sunrise (0559 CST) (an hour after the layer below) and to northerly flow by 0700 CST.

On night 3 (Fig. 5c), wind speeds between midnight and sunrise (0602 CST) were less than 4 m s^{-1} throughout the vertical profiles, and less than 1.5 m s^{-1} in the lowest 50 m AGL. Prior to midnight, higher speeds prevailed with the southerly sea breeze. Similar to night 2, the land breeze was observed earlier in the lower-level winds compared with the upper-level winds. However, on this night winds shifted abruptly from southerly flow to northerly flow, coinciding with near-adiabatic vertical temperature structures and increased NSI height as discussed earlier. The shift was most evident in the layers above 50 m AGL; below this level winds had erratic direction due to weak speeds. In the 50–100 m AGL layer, the wind shift occurred between 0200 and 0300 CST (southwest to north). From 100–150 m AGL, the winds veered between 0300 and 0330 CST (south to northwest) and from 150 to 200 m AGL, the winds backed from south to northeast between 0330 and 0500 CST. By 0600 CST, winds were northeasterly or easterly throughout the vertical profiles. While this shift was occurring, wind speeds at all heights weakened to less than 3 m s^{-1} before increasing after the shift.

On night 4 (Fig. 5d), southeasterly onshore flow dominated most of the night, unlike the other three nights. Wind speeds averaged 3.5 m s^{-1} below 100 m AGL before midnight, decreasing to 2.5 m s^{-1} between 0300 and 0600 CST. Winds generally backed to easterly between 0530 and 0830 CST, with the upper levels shifting later than the lower levels.

3.4. Spatial comparison of vertical soundings

This section compares the vertical winds at UH with those from the Ron Brown HRDL and the La Porte airport radar wind profiler. On night 1, the lidar data from the Gulf of Mexico agreed well with the UH data as the winds veered with time below 200 m AGL (Fig. 6). The lidar winds also exhibited a northwesterly land breeze first in the lower 100 m, but the timing of this (around 0500 CST) was an hour earlier than at UH. At La Porte, the wind profiles at 128 m and 186 m AGL show that a northwesterly land breeze developed between 0600 and 0700 CST (not shown); the UH winds did not turn at these levels until 0730 CST.

The night 2 lidar data at Barbour's Cut showed veering of the winds with time below 200 m AGL (Fig. 7). The lidar winds had less directional variability near the surface than UH winds because wind speeds at UH's inland location were lighter. In addition, the lidar profiles represented a mean wind over a ~3 km radius area and 3-min time period whereas the tethersonde profiles were 5-m average point measurements and thus were subject to small-scale changes in the winds. Again there was a temporal lag in wind shifts at UH versus Barbour's Cut. For example, the lower-level winds shifted from

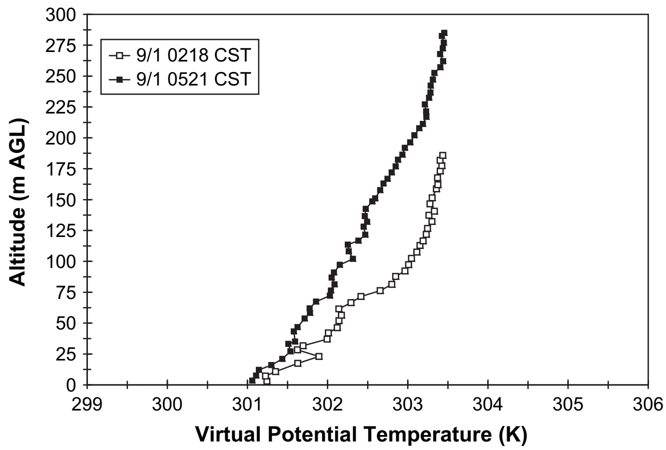

Fig. 10. Tethersonde vertical profiles of virtual potential temperature (θ_v) illustrating cooling above 50 m AGL on night 1 (August 31–September 1, 2006).

westerly to northwesterly (land breeze) in the lidar data between 0330 and 0400 CST, but not until 0500 CST at UH. The La Porte wind profiles at 128 m and 186 m AGL matched well with UH, showing west–northwesterly flow between 0500 and 0600 CST (not shown). But, a sharp wind shift to north at La Porte occurred about 0630 CST, 30 min before the UH winds at these levels.

The lidar data on night 3 from Barbour's Cut captured the rapid wind shift in the lowest 150 m AGL (from southerly to northerly/northeasterly) seen in the UH winds. The lidar winds turned first at the lower levels also, with the shift moving upward over time (Fig. 8). As at UH, the lidar winds backed in the 150–200 m layer from southeast to northeast. Interestingly, though, there was limited lag (perhaps 30 min at the most) in the timing of wind shifts between the two data sets as seen in a comparison of the lowest 200 m AGL lidar winds at 0300 CST (Fig. 8) with the 0338 CST UH winds (Fig. 5c). At La Porte, the winds backed from southeast to northeast at both the 128 m and the 186 m levels (UH backed only at 186 m) and any timing lag was small between these two locations as well (Fig. 9).

On night 4, only the La Porte data set was available for comparison and it showed southeasterly winds all night similar to UH. However, while the UH winds had a shift to the east in the 100–150 m AGL layer around 0745 CST, La Porte's winds briefly switched to easterly by 0830 CST and then returned to southeasterly within 2 h.

4. Discussion

The spatial view of the Houston area presented by these three data sets provides support for the development of a land breeze in the early morning on the first three nights. The onshore synoptic flow on the fourth night, although weak, interrupted the diurnal oscillation and a land breeze did not develop. On the land breeze nights, the northerly flow began near the coast and propagated inland horizontally and vertically with time. This idea is supported by both the turning of the winds at the lower levels first in the tethersonde and lidar data sets (followed by the layers above) as well as the delayed measurements of northerly flow at the inland UH campus versus the two coastal sites.

The third night was interesting because of the abrupt wind shift from southerly to northerly and the limited delay between shifts at the coastal locations and UH compared with the previous two nights. However, this appears to be another case of land breeze development due to two factors – the northerly flow propagated from the surface upward as on the other nights, and the data sets revealed the winds continuing to veer with time across the region to become southeasterly in the afternoon, completing the diurnal oscillation cycle. In addition, the striking change in the θ_v profiles provides evidence for mechanical turbulence and advection associated with the land breeze, potentially causing the increase in NSI height observed at this time.

Unlike night 3, the increase in NSI height during the pre-dawn hours on night 2 cannot be attributed solely to the land breeze. The height increase coincided with the land breeze, but there is limited evidence for greater mixing or advection; wind speeds decreased below 200 m AGL and the θ_v profiles had little change near the surface after the breeze commenced. On nights 1 and 4, the NSI height increase did not seem to be related to changes in wind flows at all. The wind shift occurred after the height increase on night 1, and night 4's winds were relatively constant during the period of increase. It appears that the BL temperature structure on these nights was at least partly influenced by radiational cooling. For example, Fig. 10 shows that on night 1, the atmosphere above 50 m AGL cooled more extensively than that below. These observations may provide support for results from nocturnal longwave and turbulent cooling model simulations conducted by Savijärvi (2006). Savijärvi's mid-latitude summertime simulations assumed 10-m wind speeds of less than 1–1.5 m s^{-1} and found that longwave, rather than turbulent, cooling dominated the NBL above about 1 m. Our 10-m wind speed observations matched this criterion, but our results showed limited cooling at greater heights than only 1 m. This difference may partly be attributed to the influence of urban turbulence at the UH site, while the simulations assumed a smooth homogeneous surface.

5. Summary

Through a spatial analysis of vertical winds in Houston, we have shown a diurnal wind oscillation on the three experiment nights that had weak synoptic forcing. Although the synoptically driven onshore flow on night 4 was fairly weak, it precluded the full extent of the local-scale wind cycle from developing. On the nights the land breeze developed, it began at the coastline and propagated inland over time, both horizontally and vertically, as seen in the data sets (lower-level winds turned first and the wind shifted later at the inland UH site versus the coastal sites).

A weakly stable NSI formed on all four experiment nights at the urban UH site as seen in the tethersonde vertical temperature profiles. A stronger and deeper NSI developed on nights with lighter winds and the weakest NSI occurred on the most humid night. Averaging in depth between 145 and 200 m AGL, the NSI typically formed within 2–3 h after sunset and the height remained relatively constant before increasing during the pre-dawn hours. The height increase may have been influenced by the land breeze on two of the nights, with night 3 developing near-adiabatic temperature structures below 100 m AGL after the wind shift. Longwave radiational cooling above 50 m AGL may have contributed to the NSI increase on the other nights.

Our analysis of synoptic conditions above the BL revealed no obvious correlation between NSI height and strength and upper-level subsidence, directional wind shear below 1 km, or upper-level wind flows.

Acknowledgements

We are grateful for financial support from the Texas Commission on Environmental Quality (TCEQ) and Houston Advanced Research Center. We would like to thank Bryan Lambeth (TCEQ) and Wayne

Angevine (Cooperative Institute for Research in Environmental Sciences, University of Colorado at Boulder and NOAA Earth System Research Laboratory) for providing the La Porte wind profiler data set. Special thanks go to Ryan Perna, Leo Pedemonte, Fong Ngan, Soontae Kim, HyunCheol Kim, and Xiangshang Li for data collection and analysis assistance. Two anonymous reviewers also provided valuable comments that improved this manuscript.

References

André, J.C., Mahrt, L., 1982. The nocturnal surface inversion and influence of clear-air radiative cooling. Journal of the Atmospheric Sciences 39, 864–878.

Baker, D.G., Enz, J.W., Paulus, H.J., 1969. Frequency, duration, commencement time and intensity of temperature inversions at St. Paul – Minneapolis. Journal of Applied Meteorology 8, 747–753.

Banta, R.M., Senff, C.J., Nielsen-Gammon, J., Darby, L.S., Ryerson, T.B., Alvarez, R.J., Sandberg, S.P., Williams, E.J., Trainer, M., 2005. A bad air day in Houston. Bulletin of the American Meteorological Society 86, 657–669.

Berman, S., Ku, J.Y., Rao, S.T., 1999. Spatial and temporal variation in the mixing depth over the northeastern United States during the summer of 1995. Journal of Applied Meteorology 38, 1661–1673.

Case, J.L., Wheeler, M.M., Manobianco, J., Weems, J.W., Roeder, W.P., 2005. A 7-yr climatological study of land breezes over the Florida spaceport. Journal of Applied Meteorology 44, 340–356.

Clappier, A., Martilli, A., Grossi, P., Thunis, P., Pasi, F., Krueger, B.C., Calpini, B., Graziani, G., van den Bergh, H., 2000. Effect of sea breeze on air pollution in the greater Athens area. Part I: numerical simulations and field observations. Journal of Applied Meteorology 39, 546–562.

Clarke, J.F., 1969. Nocturnal urban boundary layer over Cincinnati, Ohio. Monthly Weather Review 97, 582–589.

Dabberdt, W.F., Carroll, M.A., Baumgardner, D., Carmichael, G., Cohen, R., Dye, T., Ellis, J., Grell, G., Grimmond, S., Hanna, S., Irwin, J., Lamb, B., Madronich, S., McQueen, J., Meagher, J., Odman, T., Pleim, J., Schmid, H.P., Westphal, D.L., 2004. Meteorological research needs for improved air quality forecasting – report of the 11th prospectus development team of the U.S. weather research program. Bulletin of the American Meteorological Society 85, 563–586.

Darby, L.S., 2005. Cluster analysis of surface winds in Houston, Texas, and the impact of wind patterns on ozone. Journal of Applied Meteorology 44, 1788–1806.

Emeis, S., Türk, M., 2004. Frequency distributions of the mixing height over an urban area from SODAR data. Meteorologische Zeitschrift 13, 361–367.

Eresmaa, N., Karppinen, A., Joffre, S.M., Räsänen, J., Talvitie, H., 2006. Mixing height determination by ceilometer. Atmospheric Chemistry and Physics 6, 1485–1493.

Frehlich, R.G., Meillier, Y., Jensen, M.L., Balsley, B.B., Sharman, R., 2006. Measurements of boundary layer profiles in an urban environment. Journal of Applied Meteorology and Climatology 45, 821–837.

Godowitch, J.M., Ching, J.K.S., Clarke, J.F., 1985. Evolution of the nocturnal inversion layer at an urban and nonurban location. Journal of Climate and Applied Meteorology 24, 791–804.

Grossi, P., Thunis, P., Martilli, A., Clappier, A., 2000. Effect of sea breeze on air pollution in the greater Athens area. Part II: analysis of different emission scenarios. Journal of Applied Meteorology 39, 563–575.

Grund, C.J., Banta, R.M., George, J.L., Howell, J.N., Post, M.J., Richter, R.A., Weickmann, A.M., 2001. High-resolution Doppler lidar for boundary layer and cloud research. Journal of Atmospheric and Oceanic Technology 18, 376–393.

Ha, J.-K., Mahrt, L., 2003. Radiative and turbulent fluxes in the nocturnal boundary layer. Tellus 55A, 317–327.

Lu, R., Turco, R., 1996. Ozone distributions over the Los Angeles Basin: three-dimensional simulations with the SMOG model. Atmospheric Environment 30, 4155–4176.

Mahrt, L., André, J.C., Heald, R.C., 1982. On the depth of the nocturnal boundary layer. Journal of Applied Meteorology 21, 90–92.

Martilli, A., 2003. A two-dimensional numerical study of the impact of a city on atmospheric circulation and pollutant dispersion in a coastal environment. Boundary-Layer Meteorology 108, 91–119.

Nielsen-Gammon, J., Powell, C.L., Mahoney, M.J., Angevine, W.M., Senff, C., White, A., Berkowitz, C., Doran, C., Knupp, K., 2008. Multisensor estimation of mixing heights over a coastal city. Journal of Applied Meteorology and Climatology 47, 27–43.

Oke, T.R., 1978. Boundary Layer Climates, second ed. Routledge, London, 435 pp.

Oke, T.R., East, C., 1971. The urban boundary layer in Montreal. Boundary-Layer Meteorology 1, 411–437.

Rappenglück, B., Perna, R., Zhong, S., Morris, G.A., 2008. An analysis of the vertical structure of the atmosphere and the upper-level meteorology and their impact on surface ozone levels in Houston, Texas. Journal of Geophysical Research 113, D17315. doi:10.1029/2007JD009745.

Rotach, M.W., Vogt, R., Bernhofer, C., Batchvarova, E., Christen, A., Clappier, A., Feddersen, B., Gryning, S.E., Martucci, G., Mayer, H., Mitev, V., Oke, T.R., Parlow, E., Richner, H., Roth, M., Roulet, Y.A., Ruffieux, D., Salmond, J.A., Schatzmann, M., Voogt, J.A., 2005. BUBBLE – an urban boundary layer meteorology project. Theoretical and Applied Climatology 81, 231–261.

Savijärvi, H., 2006. Radiative and turbulent heating rates in the clear-air boundary layer. Quarterly Journal of the Royal Meteorological Society 132, 147–161.

Seibert, P., Beyrich, F., Gryning, S.E., Joffre, S., Rasmussen, A., Tercier, P., 2000. Review and intercomparison of operational methods for the determination of the mixing height. Atmospheric Environment 34, 1001–1027.

Teixeira, J., Stevens, B., Bretherton, C.S., Cederwall, R., Doyle, J.D., Golaz, J.C., Holtslag, A.A.M., Klein, S.A., Lundquist, J.K., Randall, D.A., Siebesma, A.P., Soares, P.M.M., 2008. Parameterization of the atmospheric boundary layer – a view from just above the inversion. Bulletin of the American Meteorological Society 89, 453–458.

United States Environmental Protection Agency, 2008. Fact Sheet: Final Revisions to the National Ambient Air Quality Standards for Ozone URL: <http://www.epa.gov/air/ozonepollution/pdfs/2008_03_factsheet.pdf>, 6 pp.

Vernekar, K.G., Mohan, B., Saxena, S., Patil, M.N., 1993. Characteristics of the atmospheric boundary layer over a tropical station as evidenced by tethered balloon observations. Journal of Applied Meteorology 32, 1426–1432.

Zhong, S., Takle, E.S., 1992. An observational study of sea and land-breeze circulation in an area of complex coastal heating. Journal of Applied Meteorology 31, 1426–1438.